Supplementary Information

Metal Cations Promote Coupled-Ion-Electron Transfer During Deposition and Corrosion

E. I. Stern[1], K. A. Thurman[1], F. Brito dos Santos[1], P. A. Kempler[1*]

[1]*Department of Chemistry and Biochemistry and the Oregon Center for Electrochemistry, University of Oregon, Eugene, OR, USA*

*Correspondence: pkempler@uoregon.edu

Baseline corrections for kinetic analysis

Measurements of Cu^{2+} adsorption were corrected for double-layer charging using the current measured in a non-Faradaic region (where the coverage of Cu approached zero) from E = 0.39–0.40 V for Cu^{2+}. This allowed the double layer capacitance to be directly quantified in the electrolyte containing divalent cations and was assumed to more accurately reflect the double layer charging current. No significant changes in the kinetic analysis resulted from increasing the potential region over which the double layer capacitance was calculated. Ag^{+} could not be fully desorbed from the surface prior to the onset of Au oxidation in some of the electrolytes, and so the double layer charging current was measured in the respective concentration of $HClO_4$(aq) (**Figure S19**) for Ag^{+} over the corresponding potential range.

Kinetics for Monovalent Cations (Silver):

1.0 Elementary metal transfer reaction:

We first consider a single step adsorption reaction for an aqueous Ag^+ species at a surface site, *

$$Ag_{aq}^{+} + e^{-} + * \leftrightarrow Ag^{*} \quad \text{(S1)}$$

For a monovalent surface redox reaction, the equilibrium surface potential (E_{eq}) is dependent on the ratio of the activities of reactants and products and is referenced to a formal potential ($E^{0'}$)

$$E_{eq} = E_{Ag*}^{0'} - \frac{k_b T}{e}\left[\ln\left(\frac{\Gamma_{Ag*}}{\Gamma_{*}\, a_{Ag+}}\right)\right] \quad \text{(S2)}$$

where Γ_i represents a surface activity, a_i represents the activity of a dissolved species, e is the elementary charge, k_B is Boltzmann's constant, T is temperature. The formal potential is defined for the condition where the activity of Ag^+ is 1 and the activities of the occupied and unoccupied sites are equal, which may not necessarily be accessible for all surface reactions.

When interactions between surface adsorbates are negligible, the surface activity can be expressed in terms of the fractional surface coverage, θ,

$$\theta = \Gamma_{Ag*}/\Gamma_{*}^{o} \quad \text{(S3)}$$

assuming $\Gamma_{*} + \Gamma_{Ag*} = \Gamma_{*}^{o}$ such that $\Gamma_{*}/\Gamma_{*}^{o} = (1-\theta)$. The apparent rate of the adsorption reaction, r_{app},

$$r_{app} = r_{ox} - r_{red} \quad \text{(S4)}$$

is expressed for an exchange of two elementary, first order reactions. The rate of oxidation, in this case the adsorbed silver being oxidized to an aqueous silver cation, is dependent on the number of adsorbed Ag* and the rate constant for oxidation (equation S5).

$$r_{ox} = k_{ox}\Gamma_{Ag*} \quad \text{(S5)}$$

where r_{ox} and k_{ox} are the rate of oxidation and the rate constant for oxidation, respectively with similar terms defined for the reduction reaction. The rate of the aqueous silver cation being reduced to adsorbed silver is dependent on the number of available sites for adsorption to occur, the activity of Ag^+, and the rate constant for reduction (equation S6).

$$r_{red} = k_{red}\Gamma_{*}\, a_{Ag+} \quad \text{(S6)}$$

We next assume that the rate constant for adsorption/desorption of an ion is exponentially dependent on the difference in energy between the reactants and a transition state, and that this energy varies with the applied electrochemical potential.[1]

$$k = A\exp\left(\frac{-\Delta G^{\ddagger}}{RT}\right) \tag{S7}$$

where k is the rate constant, A is the frequency factor, and $\Delta G^{\ddagger}$ is the free energy difference of the reactant and transition state. Following Butler-Volmer kinetics, the barrier height r_{red} and r_{red} are assumed to vary with the applied potential as:

$$\Delta G_{ox}^{\ddagger} = \Delta G_{0,ox}^{\ddagger} + \alpha F\left(E - E^{0'}\right) \tag{S8}$$

$$\Delta G_{red}^{\ddagger} = \Delta G_{0,red}^{\ddagger} - (1-\alpha)F\left(E - E^{0'}\right) \tag{S9}$$

Where α is a transfer coefficient that describes how the applied potential impacts the free energy of the transition state and E is the applied potential. Applying these expressions to the rate constant expression we obtain:

$$k_{ox} = A_{ox}\exp\left(\frac{-\Delta G_{0ox}^{\ddagger}}{RT}\right)\exp\left(\frac{\alpha F\left(E - E^{0'}\right)}{RT}\right) \tag{S10}$$

$$k_{red} = A_{red}\exp\left(\frac{-\Delta G_{0red}^{\ddagger}}{RT}\right)\exp\left(\frac{-(1-\alpha)F\left(E - E^{0'}\right)}{RT}\right) \tag{S11}$$

We next introduce a standard rate constant, $k^0 = A\exp((-\Delta G^{\ddagger})/\text{RT})$, leading to

$$k_{ox} = k^0\exp\left(\frac{\alpha e\left(E - E^{0'}\right)}{k_b T}\right) \tag{S12}$$

$$k_{red} = k^0\exp\left(\frac{-(1-\alpha)e\left(E - E^{0'}\right)}{k_B T}\right) \tag{S13}$$

Substituting equations S12-S13 into equations S4-S6 yields a r_{app}-E relationship.

$$r_{app} = k^0\left(\Gamma_{Ag*}\exp\left[\frac{\alpha e\left(E - E^{0'}\right)}{k_B T}\right] - \Gamma_* a_{Ag^+}\exp\left[-\frac{(1-\alpha)e\left(E - E^{0'}\right)}{k_B T}\right]\right) \tag{S14}$$

Because $E^{0'}$ is not easily measured for adsorption reactions, the apparent rate was measured with respect to the equilibrium potential for a fixed coverage of Ag^+ and is expressed as a function of a surface overpotential, ξ.[2]

$$\xi = E - E_{eq} = \left(E - E^{0'}\right) - \left(E_{eq} - E^{0'}\right) \tag{S15}$$

Substitution of equation S2 into S10 yields the surface overpotential corrected for changes in coverage and dissolved activity of Ag^+.

$$\left(E - E^{0'}\right) = \xi - \frac{k_B T}{e} \ln\left(\frac{\Gamma_{Ag*}}{a_{Ag+}\Gamma_*}\right) \tag{S16}$$

This expression can be substituted into equation S14 to yield a generalizable $r_{app}(\xi)$ expression for a univalent metal depositing with an undefined transfer coefficient.

$$r_{app} = k^0\left(\Gamma_{Ag*}\left(\frac{\Gamma_{Ag*}}{a_{Ag+}\Gamma_*}\right)^{-\alpha}\exp\left[\frac{\alpha e(\xi)}{k_B T}\right] - \Gamma_* a_{Ag} + \left(\frac{\Gamma_{Ag*}}{a_{Ag+}\Gamma_*}\right)^{1-\alpha}\exp\left[-\frac{(1-\alpha)e\xi}{k_B T}\right]\right) \tag{S17a}$$

$$r_{app} = k_0 \Gamma_{Ag*}^{1-\alpha}\left(a_{Ag+}\Gamma_*\right)^{\alpha}\left(\exp\left[\frac{\alpha e\xi}{k_B T}\right] - \exp\left[-\frac{(1-\alpha)e\xi}{k_B T}\right]\right) \tag{S17b}$$

which can be expressed in terms of a fractional surface coverage using equation S3

$$r_{app} = k_0 a_{Ag+}^{\alpha}\Gamma_*^{o}\theta^{1-\alpha}(1-\theta)^{\alpha}\left(\exp\left[\frac{\alpha e\xi}{k_B T}\right] - \exp\left[-\frac{(1-\alpha)e\xi}{k_B T}\right]\right) \tag{S18}$$

The self-exchange rate, r_0, for Ag^+ on the surface is defined as the rate at $E = E_{eq}$ (ξ=0)

$$r_0 = k_0 \Gamma_*^{o}\theta^{1-\alpha}(1-\theta)^{\alpha} a_{Ag+}^{\alpha} \tag{S19}$$

The predicted reaction order for r_0 with respect to aqueous silver at a fixed coverage is α, where the value of α can be determined from the potential-dependent rate at high driving force and/or the apparent reaction order for r_0 on fractional surface coverage. The observed reaction order for a_{Ag+} is inconsistent with the apparent α (0.5) measured for Ag^+.

1.1 Metal assisted desolvation prior to transfer:

Generally, the increased reaction order for r_0 with respect to a_{Ag^+} indicates a promoting effect of aqueous Ag^+ on the metal transfer reaction. One possible mechanism for ion transfer that is consistent with a reaction order ~1 for Ag^+ includes solvent transfer between adjacent Ag^+ cations (equation S15)

$$2\,Ag^+(H_2O)_n \leftrightarrow Ag^+(H_2O)_{n+1} + Ag^+(H_2O)_{n-1} \tag{S20}$$

where the interfacial ion transfer step remains the rate determining step

$$Ag^+(H_2O)_{n-1} + e^- + * \leftrightarrow Ag^* + (n-1)H_2O \tag{S21}$$

and the activity of the partially de-solvated species is

$$a_{Ag(H2O)n-1} = K_s \frac{\left(a_{Ag(H2O)n}\right)^2}{a_{Ag(H2O)n+1}} \tag{S22}$$

The kinetics of self-exchange can be described as

$$r_{ox} = k_{ox}\Gamma^{o}_{*}\theta a^{(n-1)}_{H_2O} \quad \text{(S23)}$$

$$r_{red} = k_{red}K_s(1-\theta)\left(a_{Ag(H2O)n}\right)^2\left(a_{Ag(H2O)n+1}\right)^{-1} \quad \text{(S24)}$$

Substituting these reactants and products into equation S13 yields

$$r_{app} = k_0 K_s^{\alpha}\Gamma^{o}_{*}\theta^{1-\alpha}(1-\theta)^{\alpha}a^{2\alpha}_{Ag(H2O)n}a^{(n-1)\alpha}_{H_2O}a^{-\alpha}_{Ag(H2O)n+1}\left(\exp\left[\frac{\alpha e\xi}{k_BT}\right] - \exp\left[-\frac{(1-\alpha)e\xi}{k_BT}\right]\right) \quad \text{(S25)}$$

From this the exchange rate can be expressed as

$$r_0 = k_0 K_s^{\alpha}\Gamma^{o}_{*}\theta^{1-\alpha}(1-\theta)^{\alpha}a^{2\alpha}_{Ag(H2O)n}a^{(n-1)\alpha}_{H_2O}a^{-\alpha}_{Ag(H2O)n+1} \quad \text{(S26)}$$

Which is consistent with a reaction order ~ 1 with respect to Ag^+(aq) as well as the measured α = 0.5 and corresponding coverage dependence. However, if the moles of $^{Ag^+(H_2O)_{n+1}}$ are directly related to $^{Ag^+(H_2O)_{n-1}}$ and reside in the same ensemble (such that the activities are directly related), this expression collapses to the original reaction order equal to α. One possible explanation is that the activated metal complex ($Ag^+(H_2O)_{n-1}$) is weakly adsorbed whereas the species transferring a solvent molecule is in rapid exchange with the bulk $Ag(H_2O)_n$ reactant.

1.2 Pre-adsorption prior to transfer reaction(s):

The overall process of metal transfer likely includes pre-adsorbed Ag^+ species within the double layer,[3,4] where the surface activity of Ag^+ may be greater/lesser than the activity of Ag^+ in free solution.

$$Ag^+ \leftrightarrow Ag^+_s \quad \text{(S27)}$$

And the rate determining step is still described as an elementary transfer from the pre-adsorbed species.

$$Ag^+_s + e^- + * \leftrightarrow Ag^* \quad \text{(S28)}$$

Chemical (potential-independent) adsorption is indistinguishable from elementary metal ion transfer on the basis of the measured transfer coefficient and reaction orders. The kinetics are expressed as

$$r_{ox} = k_{ox}\theta\Gamma_{Ag^+_s} \quad \text{(S29)}$$

$$r_{red} = k_{red}(1-\theta)\Gamma_{Ag*} \quad \text{(S30)}$$

where $\Gamma_{Ag^+_s}$ is the surface excess activity of non-specifically adsorbed Ag^+. When the pre-adsorption step is not rate limiting, the surface activity of the pre-adsorbed species can be related

to the dissolved activity of Ag^+ by an equilibrium constant $\Gamma_{Ag^+_s} = K_a a_{Ag^+}$, and following a similar set of steps used to obtain equation S18 yields

$$r_{app} = k_0 K_a^{\alpha} \Gamma_*^{o} \theta^{1-\alpha} (1-\theta)^{\alpha} a_{Ag^+}^{\alpha} \left(\exp\left[\frac{\alpha e \xi}{k_b T}\right] - \exp\left[\frac{-(1-\alpha) e \xi}{k_b T}\right] \right) \quad \text{(S31)}$$

Which yields a similar set of reaction orders to equation S13. The role of pre-adsorption could in principle be resolved based on the temperature dependence of k_0 and K_a as well as independent measurements of $\Gamma_{Ag^+_s}$.

1.3 Interaction energy and non-ideal adsorption isotherms during transfer

When the interaction energy between adsorbates cannot be ignored, one possible solution is a linear correction to the Langmuir isotherm, originally proposed by Frumkin

$$k_{red} a_{Ag^+} (1-\theta) = k_{ox} \theta e^{g\theta} \quad \text{(S33)}$$

Which implies a modified expression for the equilibrium surface potential

$$E_{eq} = E^{0'} - \frac{k_b T}{e}\left[\ln\left(\frac{\theta}{(1-\theta)\, a_{Ag^+}}\right) + g\theta\right] \quad \text{(S34)}$$

Substitution into equation S15 yields a similar expression for the surface overpotential

$$\left(E - E^{0'}\right) = \xi - \frac{k_B T}{e}\left[\ln\left(\frac{\Gamma_{Ag*}}{a_{Ag^+}\Gamma_*}\right) + g\theta\right] \quad \text{(S35)}$$

An additional term could be introduced that accounts for interactions between the adsorbed silver and the transition state complex, $g^{\ddagger}$:

$$k_{ox} = k^0 \exp\left(\frac{\alpha e\left(E - E^{0'}\right)}{k_b T} + \alpha g^{\ddagger} \theta\right) \quad \text{(S36)}$$

$$k_{red} = k^0 \exp\left(\frac{-(1-\alpha) e\left(E - E^{0'}\right)}{k_B T} - (1-\alpha) g^{\ddagger} \theta\right) \quad \text{(S37)}$$

Which leads to a modified r_{app}-ξ expression after substitution into equation S4-S6

$$r_{app} = k^0 \left(\Gamma_{Ag*} \exp\left[\frac{\alpha e \xi}{k_B T} + \alpha g^{\ddagger} \theta\right] / \exp\left[\alpha \ln\left(\frac{\theta}{a_{Ag^+}(1-\theta)}\right) + \alpha g \theta\right] - \Gamma_* a_{Ag^+} \exp\left[-\frac{(1-\alpha)}{k_B}\right.\right.$$

$$r_{app} = k_0 a_{Ag^+}^{\alpha} \Gamma_*^{o} \theta^{1-\alpha} (1-\theta)^{\alpha} \exp\left[\frac{g^{\ddagger}}{g}\right] \left(\exp\left[\frac{\alpha e \xi}{k_B T}\right] - \exp\left[-\frac{(1-\alpha) e \xi}{k_B T}\right] \right) \quad \text{(S38)}$$

However, when $g^{\ddagger} \sim g$, indicating that interactions between adsorbates is similar interactions with the transition state, the resulting rate expression is indistinguishable from equation S18.

Kinetics for Divalent Cations (Copper):

2.0 Rate determining metal transfer to adsorbed Cu^{+}:

Cu deposition and corrosion have been reported to occur via a set of sequential charge transfer steps where the formation of an unstable Cu^{+} intermediate is assumed to be the RDS.[5,6] If the Cu^{+} species is stabilized by an adsorption site, the reaction can be expressed as

$$Cu^{2+} + e^{-} + * \leftrightarrow Cu^{+*} \quad \text{(S39)}$$

$$Cu^{+*} + e^{-} \leftrightarrow Cu^{*} \quad \text{(S40)}$$

and the forward and backwards rates for the RDS are similar in form to those derived for Ag^{+}

$$r_{ox} = k_{ox}\Gamma_{Cu+*} \quad \text{(S41)}$$

$$r_{red} = k_{red}\Gamma_{*}a_{Cu2+} \quad \text{(S42)}$$

leading to a similar expression for the apparent rate

$$r_{app} = k_0 a_{Cu2+}^{\alpha}\Gamma_{*}^{o}\theta^{1-\alpha}(1-\theta)^{\alpha}\left(\exp\left[\frac{\alpha e\xi}{k_B T}\right] - \exp\left[-\frac{(1-\alpha)e\xi}{k_B T}\right]\right) \quad \text{(S43)}$$

and self-exchange rate

$$r_0 = k_0\Gamma_{*}^{o}\theta^{1-\alpha}(1-\theta)^{\alpha}a_{Cu^{2+}}^{\alpha} \quad \text{(S44)}$$

2.1 Metal assisted desolvation prior to reductive adsorption

Following a similar approach derived for univalent Ag^{+} transfer, we consider a metal-assisted change in coordination for Cu^{2+} prior to metal ion transfer.

$$2\,Cu^{2+}(H_2O)_n \leftrightarrow Cu^{2+}(H_2O)_{n+1} + Cu^{2+}(H_2O)_{n-1} \quad \text{(S54)}$$

where the interfacial ion transfer step remains, the rate determining step

$$Cu^{2+}(H_2O)_{n-1} + e^{-} + * \leftrightarrow Cu^{+*} + (n-1)H_2O \quad \text{(S55)}$$

This leads to a similar rate expression which leads to $m = 1$ for Cu^{2+} when $\alpha = 0.5$

$$r_{app} = k_0 K_s^{\alpha}\Gamma_{*}^{o}\theta^{1-\alpha}(1-\theta)^{\alpha}a_{Cu(H2O)n}^{2\alpha}a_{H_2O}^{(n-1)\alpha}a_{Cu(H2O)n+1}^{-\alpha}\left(\exp\left[\frac{\alpha e\xi}{k_B T}\right] - \exp\left[-\frac{(1-\alpha)e\xi}{k_B T}\right]\right) \quad \text{(S56)}$$

Estimated impacts of nearest neighbor interactions:

An idealized Au(111) surface presents two sets of three-fold hollow sites and (Σ_I, Σ_J) with only one set being occupied at complete coverage of the surface. The total number of sites available for adsorption at $\theta = 0$ is $\Sigma_I + \Sigma_J$. An adsorbate in Σ_I physically obstructs one site in Σ_I, three sites in Σ_J, and provides six nearest-neighbor interactions (**Scheme S1**). Thus, four sites are assumed to be physically obstructed by each adsorbate whereas ten sites are assumed to be directly affected.

The probability, P, of the next adsorption site *not* being affected by previously adsorbed species is

$$P = \left(1 - \frac{L}{N}\right)^{\theta N} \tag{S57}$$

where L represents the number of impacted sites per adsorbate and N represents the number of available sites. When N is large with respect to L, this expression can be approximated using a Maclaurin series for ln(1+x)

$$\ln P = \theta N \ln\left(1 - \frac{L}{N}\right) \sim -\theta L \tag{S58}$$

such that P is approximated as

$$P \sim e^{-\theta L} \tag{S59}$$

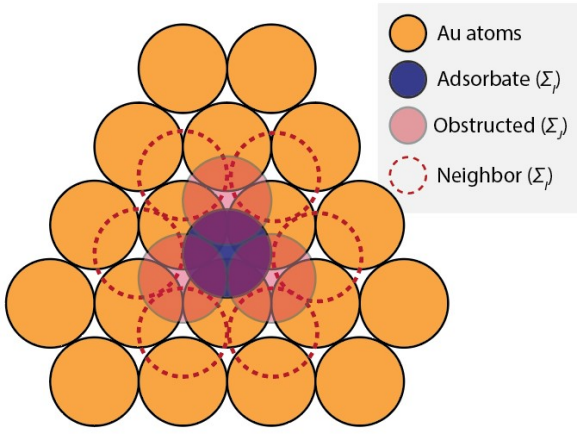

Scheme S1: Graphical representation of the interactions between an adsorbate and three-fold hollow sites on an Au(111) surface

Stepwise Instructions for Preparing Au(111) Electrodes for UPD

1. A cleaned 25 mL three-neck flask was filled with 25 mL of electrolyte and two of the three openings were sealed from the lab atmosphere.

2. A glass tube, cleaned in a consistent manner to the electrochemical cell, was suspended using a loose stopper and submerged in the solution. Then, Ar was steadily bubbled through the cell for at least 15 minutes.
3. High purity Cu or Ag wires served as the reference electrodes and were rinsed with 10 % v/v nitric acid to remove native oxide layers. A Pt wire was similarly cleaned with nitric acid and then flame cleaned with a butane torch to remove impurities from the surface
4. A polycrystalline Au thin film was gently annealed under the butane flame for 3–8 minutes until the surface slightly deepens in color. Carful control was required to heat the electrode in the reducing portion of the flame. The electrode was frequently allowed to cool, which prevented excess stress on the glass substrate leading to delamination of the Au film.
5. A fritted glass pipette was rinsed with the Ar-purged electrolyte in triplicate and then filled with the same solution. The reference electrode was then placed in this fritted pipette.
6. The Ar gas line was temporarily disconnected; the platinum wire was placed in a separate neck of the cell and connected to the potentiostat. Then, a glass or plastic piece of tubing was inserted adjacent to the Pt wire and suspended above the solution. A gentle flow of Ar blanketed the headspace of the cell.
7. The annealed Au electrode was inserted into the cell but not immediately introduced to the electrolyte to allow the surface to cool under Ar atmosphere. The Au film was connected to the potentiostat using an alligator clip touching a narrow Au band which extended away from the electrolyte.
8. After 20–30 seconds, the Au film was lowered into the solution to the top of the disk diameter.
9. Potentiostatic Electrochemical Impedance Spectroscopy (PEIS) data were collected from 200 kHz to 200 mHz with an amplitude of 10 mV and a potential offset corresponding to non-faradic potential window (either 0.60 V or 0.40 V vs E_{rev} for Cu or Ag, respectively). The cell resistance was recorded as the real impedance occurring at the minimum value for the imaginary impedance.
10. To verify the crystallinity and reversibility of the Au(111) surface, a CV (typically 25 mV/s) with manual *iR* (MIR) correction at 85% compensation using the resistance found in [9] was collected from 0.00 – 0.60 V vs E_{rev}, with an initial potential of 0.60. Repeated cleaning, annealing, and voltammetry was occasionally required to obtain a voltametric response which matched the literature.
11. Kinetically controlled data were collected using scan rates initially as high as 100 V/s and scan rates were collected in decreasing order. Electrodes in Cu-containing solutions were stable, allowing many scan rates to be collected for a single sample whereas fewer scan rates were collected for Ag-containing solutions.

Specific instructions for Ag electrodes

12. For Ag-containing electrolytes an initial CV with MIR was used to verify the crystallinity and quality of the surface like that of Cu run over the potential range 0.000–0.585 V vs E_{rev}, with an initial potential of 0.585. Electrodes which yielded inconsistent voltammetry data over this region were immediately discarded and a new Au thin film is annealed.
13. Once the electrode quality is confirmed, the resistance of the electrolyte was measured with PEIS, the electrode was held at 0.300 V vs E_{rev} for 10 seconds, and finally linear sweep voltammetry (LSV) was conducted from 0.3 to 0.585 V vs E_{rev}. The potential was held at 0.300 V before each successive scan and the scan rates were 50, 15, 2.5, 0.250, 0.050 V/s for 10 mM Ag^+ and 25, 10, 1, 0.1, 0.025 V/s for lower concentrations.

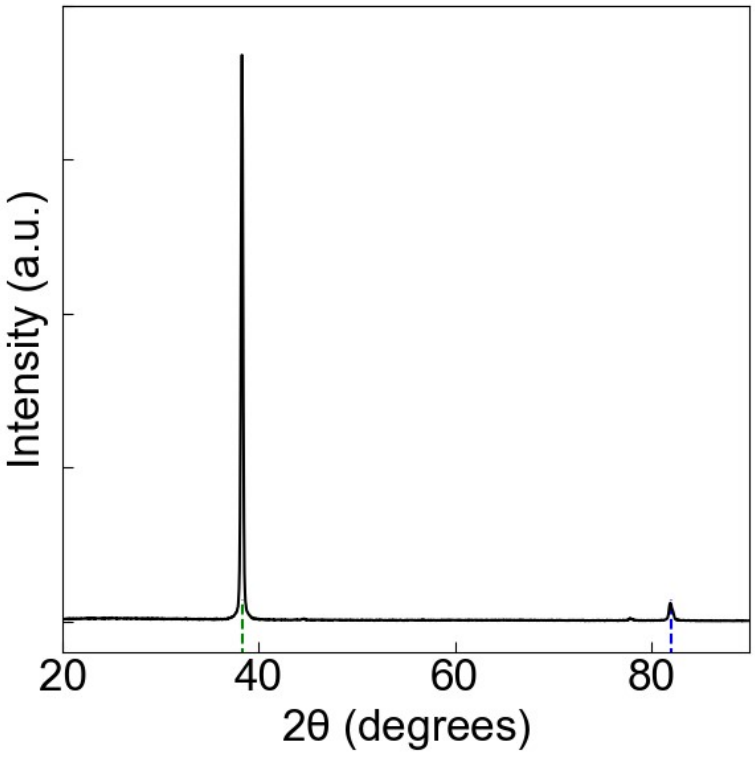

Figure S1: X-ray diffraction of a thermally evaporated flame Au thin film after annealing. The green and blue dotted lines indicate the angles of the (111) and (222) reflections, respectively. A small peak at 77.7^{o} was assigned to a (311) reflection accounting for <1% of signal.

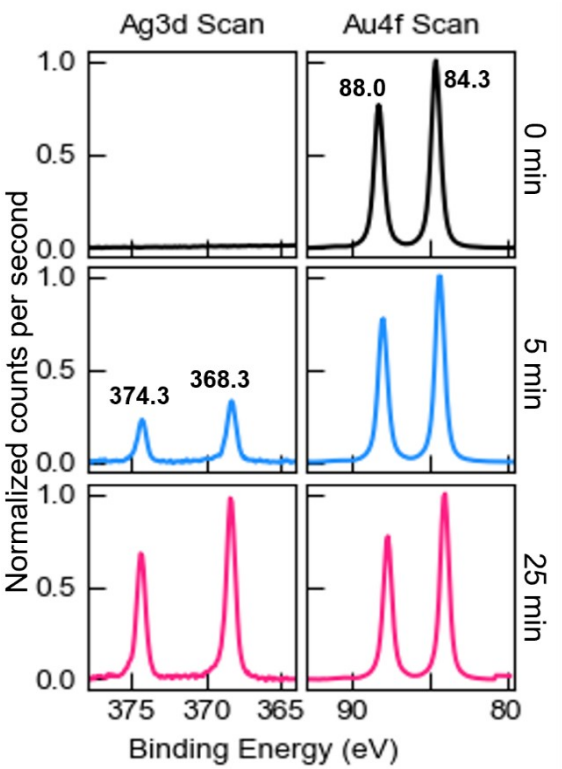

Figure S2: High resolution X-ray photoelectron spectroscopy (XPS) of an annealed Au(111) electrode after 0 minutes (black), 5 minutes (blue), and 20 minutes (pink) of cycling in an Ag^+ electrolyte. All surfaces were subjected to brief sputtering with Ar^+ which was estimated to remove the top 3 nm of material.

Table S1: Measured composition (atom %) from high resolution X-ray photoelectron spectroscopy (XPS) of an annealed Au(111) electrode after briefly sputtering the surface with Ar^+ under high vacuum. Samples were measured before (0 min) and after 5 min and 25 min of cycling in a solution containing Ag^+. Chloride impurities were assigned to the decomposition of ClO_4^-.

Element (Region)	*0 min*	*5 min*	*25 min*
Au (Au4f)	44.8	37.1	33.7
Ag (Ag3d)	-	1.33	3.92
Ti (Ti2p)	10.6	14.5	13.6
C (C1s)	12.4	9.01	7.71
O (O1s)	32.2	38.1	38.0
Cl (Cl2p)	-	-	3.20

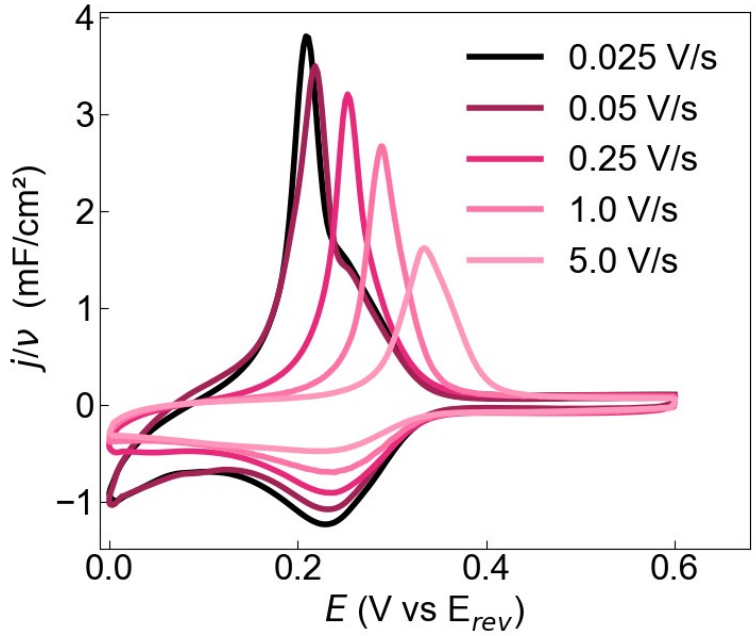

Figure S3: CV of Au(111) in 0.003 M $Cu(ClO_4)_2$ and 0.094 M $HClO_4$ (0.10 M ClO_4^-) normalized to scan-rate (ν = 0.025, 0.05, 0.25, 1, 5, V s^{-1}).

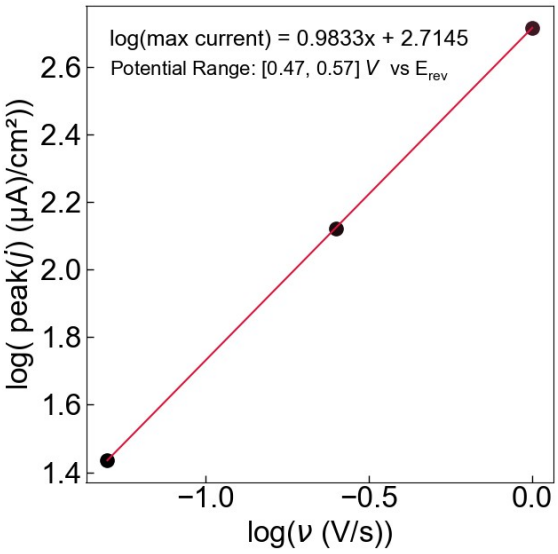

Figure S4: (a) Log-log plot comparing the peak current for Au(111) in 0.003 M $AgClO_4$ and 0.097 M $HClO_4$ (0.10 M ClO_4^-) versus scan rate (v = 0.05, 0.25, 1, s^{-1}). The red line represents the fit for the equation $\log(i=bv^a)$.

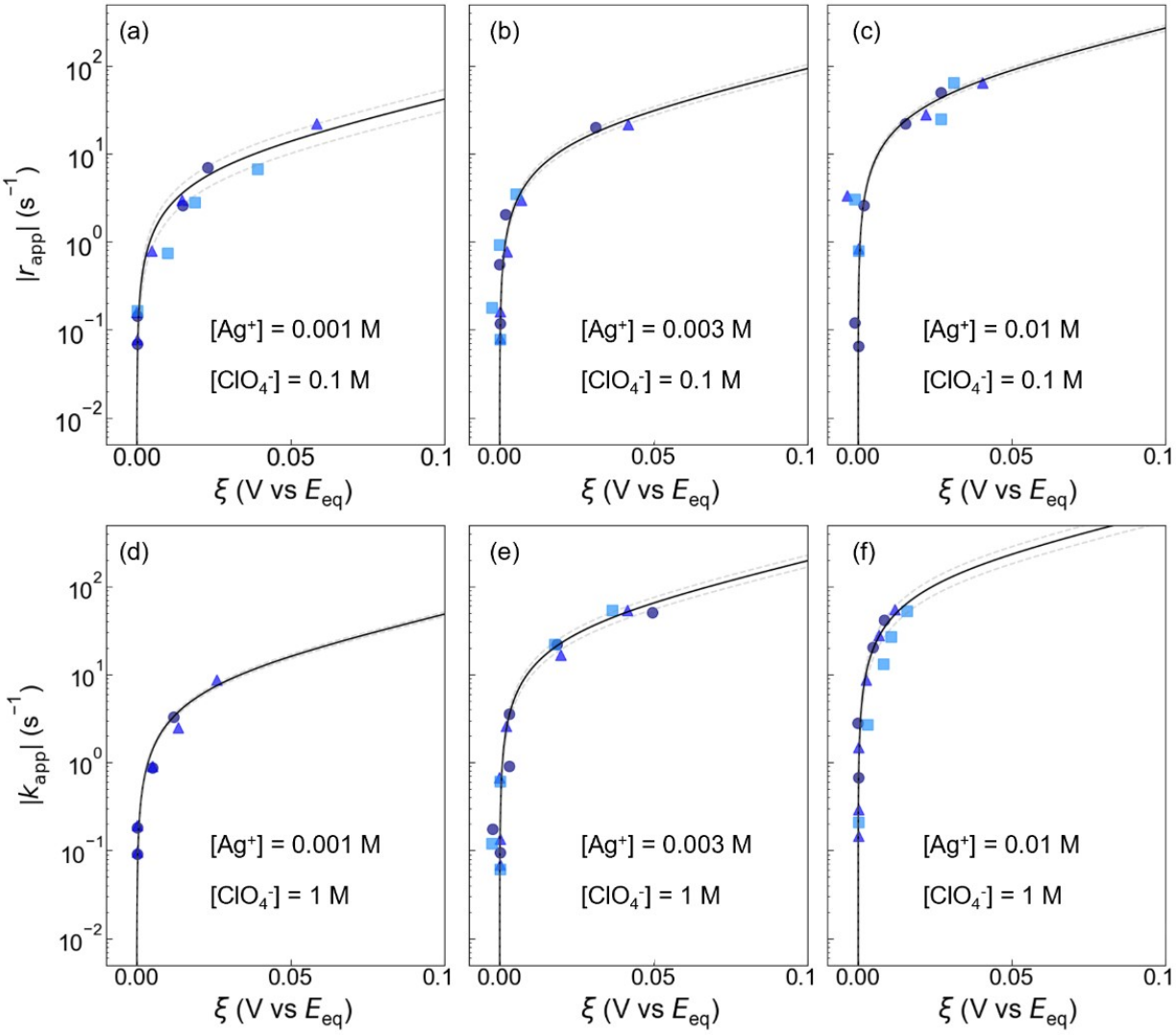

Figure S5: The apparent interfacial ion transfer rate (r_{app}) of Ag^+ as a function of adsorption overpotential (ξ) at θ_{Ag} = 0.05 in 0.1 M ClO_4^- for (a) 0.001 M Ag^+ (29 ± 8 s^{-1}), (b) 0.003 M Ag^+ (57 ± 9.8 s^{-1}), (c) 0.01 M Ag^+ (170 ± 13 s^{-1}), and in 1 M ClO_4^- for (d) 0.001 M Ag^+ (30 ± 2 s^{-1}), (e) 0.003 M Ag^+ (130 ± 8 s^{-1}), (f) 0.01 M Ag^+ (470 ± 99 s^{-1}). The different markers and shades of blue represent the different experimental trials, the black line represents the average line of best fit, and dashed lines represent the standard deviation.

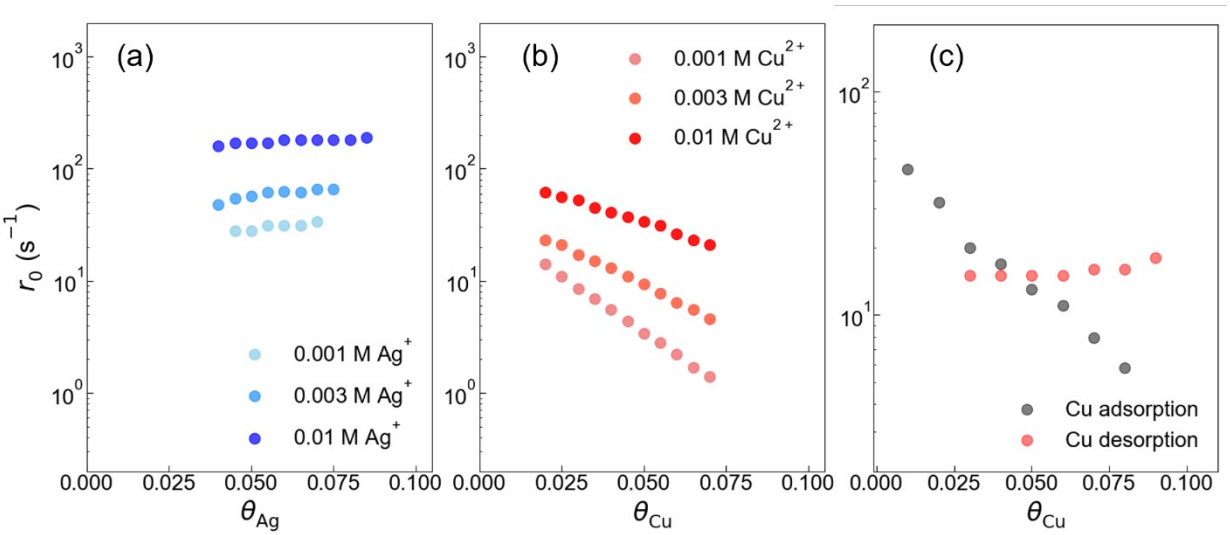

Figure S6: Coverage dependence of r_0 for Au(111) (a) Ag^+ in 100 mM ClO_4^- measured using the potential hold and desorption, (b) Cu^{2+} in 100 mM ClO_4^- using the CV and adsorption, and (c) the adsorption (grey) and desorption (orange) techniques for 1 mM Cu^{2+} in 100 mM SO_4^{2-}.

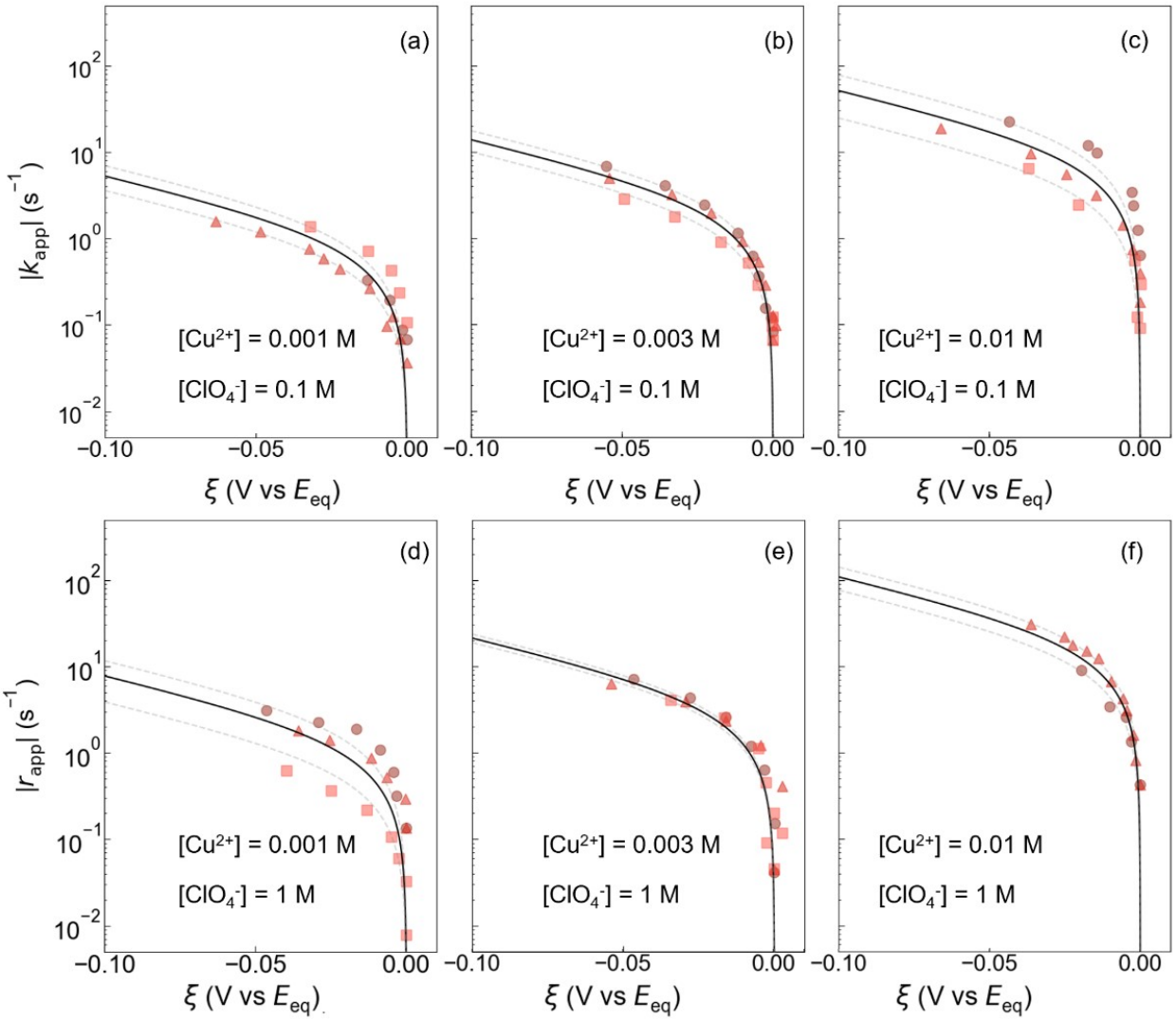

Figure S7: The apparent interfacial ion transfer rate (r_{app}) of Cu^{2+} as a function of adsorption overpotential (ξ) at θ_{Cu} = 0.05 in 0.1 M ClO_4^- for (a) 0.001 M Cu^{2+} (3.5 ± 1 s^{-1}), (b) 0.003 M Cu^{2+} (9 ± 3 s^{-1}), (c) 0.01 M Cu^{2+} (34 ± 18 s^{-1}), and in 1 M ClO_4^- for (d) 0.001 M Cu^{2+} (5 ± 3 s^{-1}), (e) 0.003 M Cu^{2+} (14 ± 2 s^{-1}), (f) 0.01 M Cu^{2+} (73 ± 22 s^{-1}). The different markers and shades of orange represent the different experimental trials, the black line represents the average line of best fit, and dashed lines represent the standard deviation.

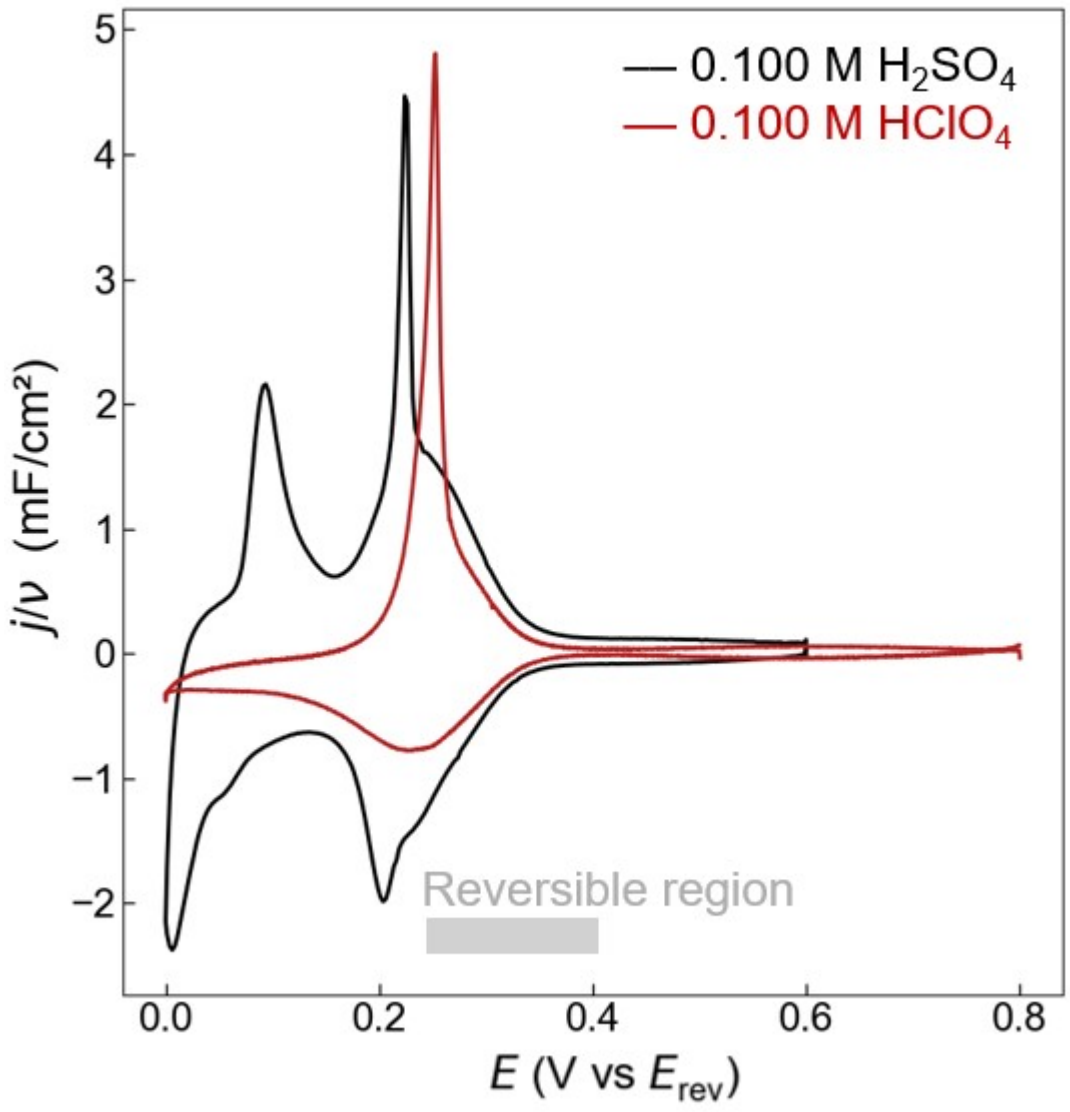

Figure S8: CV of 1 mM CuO dissolved in 0.1 M of the respective supporting electrolyte on Au(111) at 25 mV s^{-1}. The charge positive of the sharp anodic peak at around 0.2 V vs E_{rev} is what is used if desorption kinetics are being studied.

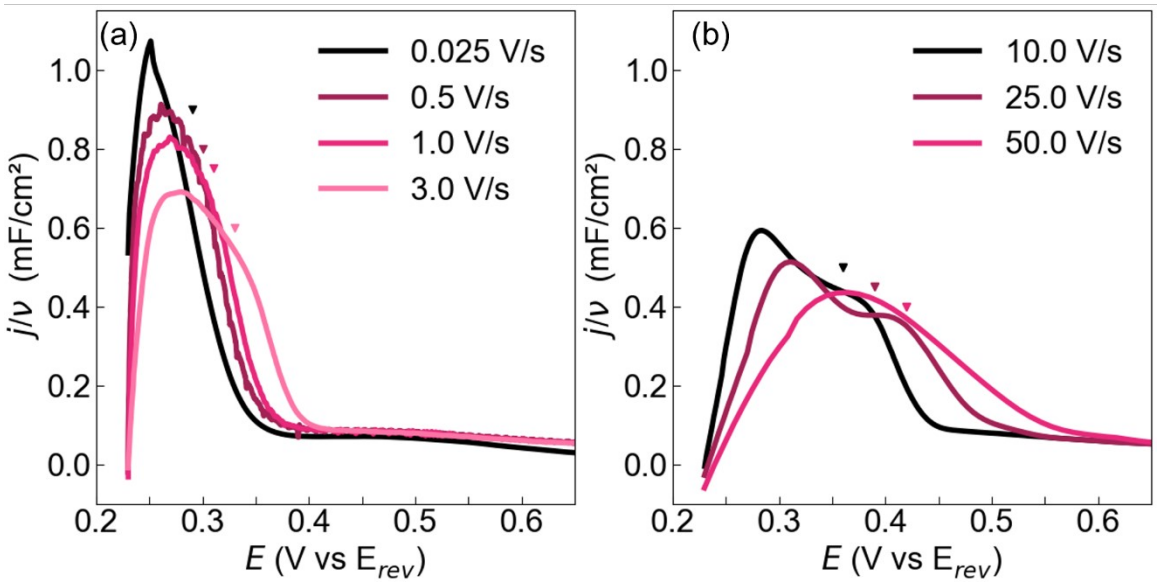

Figure S9: (a) LSV of Au(111) in 0.001 M $Cu(SO_4)_2$ and 0.098 M H_2SO_4 (0.10 M SO_4^{2-}) in the Cu UPD reversible region normalized to scan-rate (ν = 0.025, 0.5, 1, 3 V s^{-1}) for slow scan rates. (b) LSV in the same solution as (a) for fast scan-rates (ν = 10, 25, 50 V s^{-1}). Both (a) and (b) start positive of the first phase transition. The triangle markers represent the point at which $\theta = 0.05$ for the respective color in the respective plot.

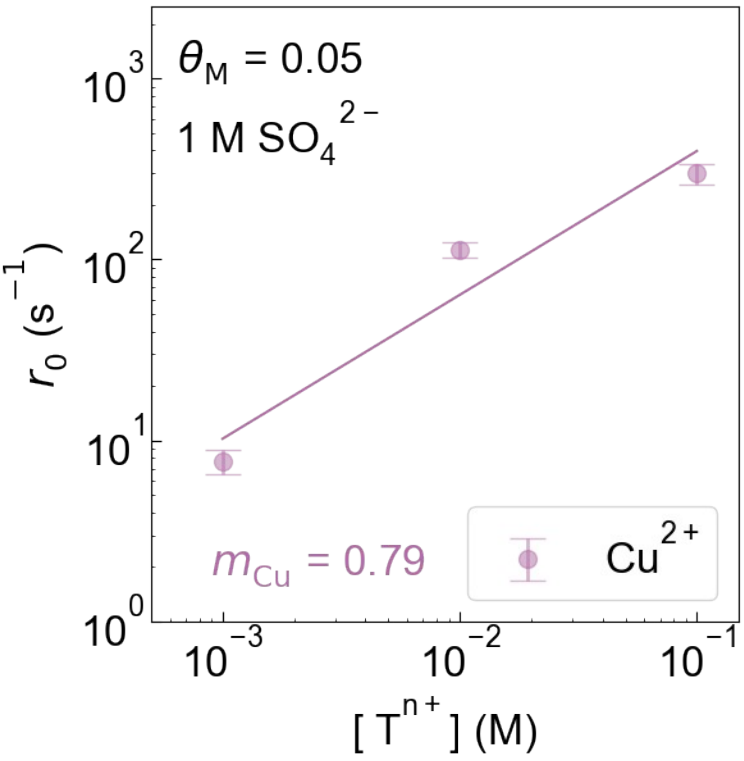

Figure S10: Dependence of the equilibrium exchange rate *(r_0)* of the metal cation vs the concentration of the respective metal cation ([T^{n+}] = 0.001, 0.01, 0.1 M) at 5% coverage in 1.00 M H_2SO_4. (a) The purple circle symbols represent experimental data whereas the solid-colored lines represent the reaction order of the rates with respect to concentration of Cu^{2+} .

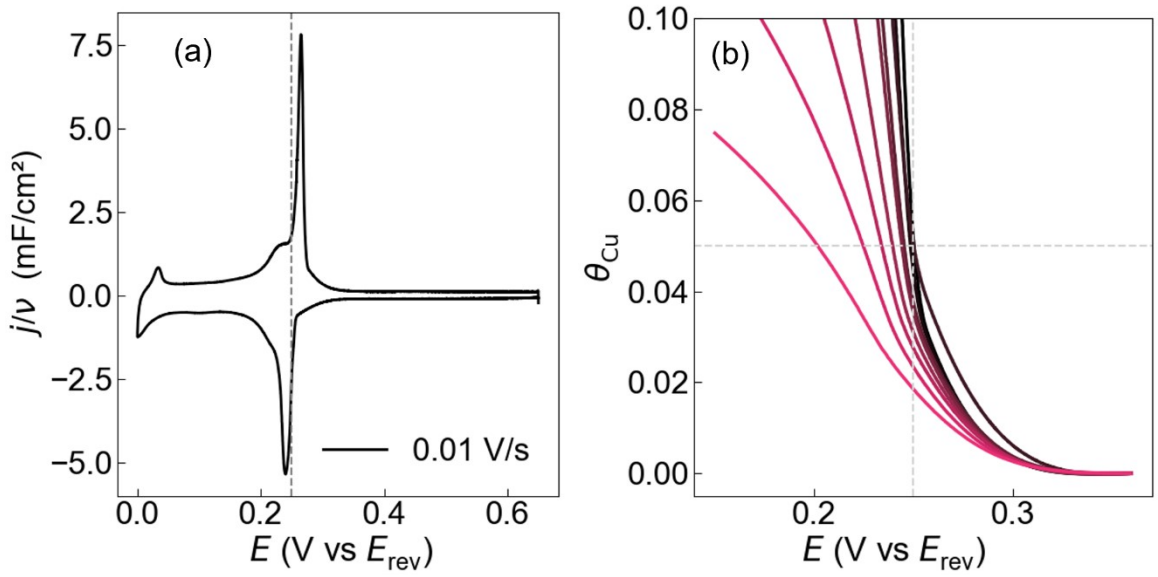

Figure S11: (a) CV of 1 mM CuO in 10 M H_2SO_4 on Au(111) normalized to a scan rate of ν = 0.01 V s^{-1} versus the reversible deposition potential of copper in the given electrolyte. (b) θ_{Cu}-E response for ν = 0.01, 0.025, 0.05, 0.075, 0.1, 0.25, 0.5, 1, 2.5 V s^{-1}, color transition from black to red as ν increases. The grey dashed lines in (a,b) show the solution for E when θ_{Cu} = 0.05 during the negative potential sweep.

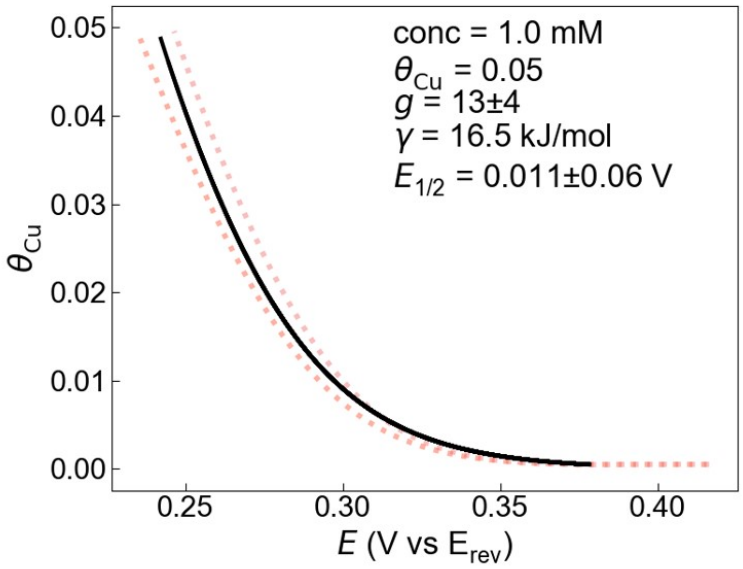

Figure S12: Adsorption isotherm fit to the Frumkin adsorption isotherm of Cu coverage vs the reversible deposition potential at 1 mM Cu^{2+} in 0.01 M ClO_4^-. The dotted red lines represent experimental data and the black line represents the line of best fit.

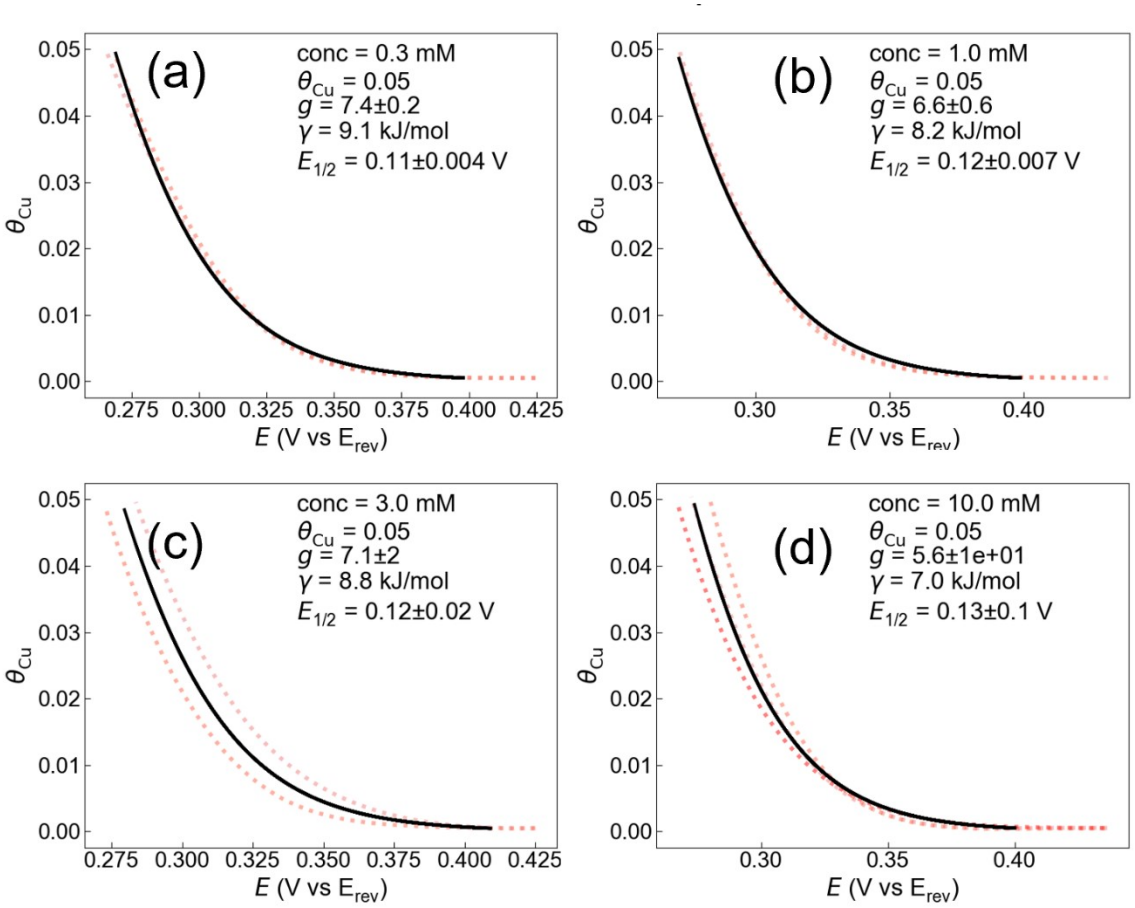

Figure S13: Potential dependent adsorption isotherm fit to the Frumkin adsorption isotherm of Cu coverage at various Cu^{2+} concentrations in 0.1 M ClO_4^-. The dotted red lines represent experimental data and the black line represents the line of best fit.

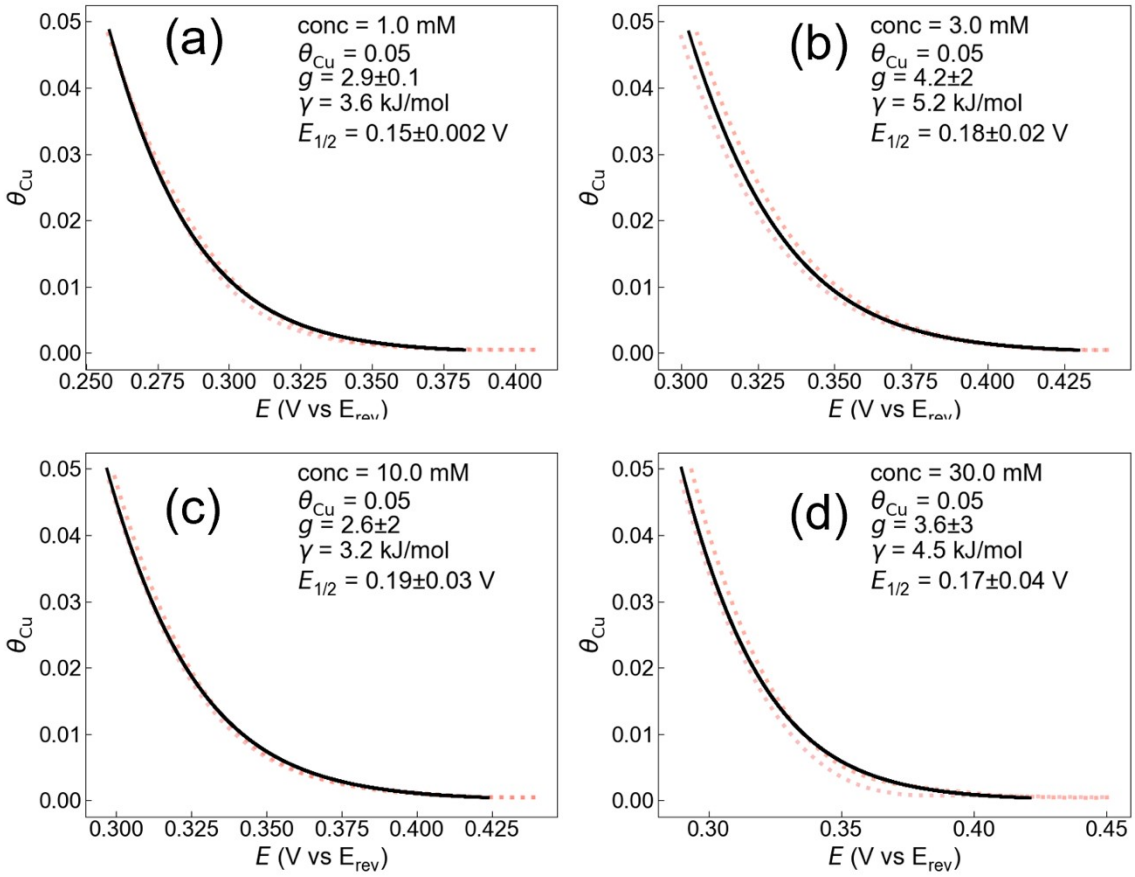

Figure S14: Potential dependent adsorption isotherm fit to the Frumkin adsorption isotherm of Cu coverage at various Cu^{2+} concentrations in 1.0 M ClO_4^-. The dotted red lines represent experimental data and the black line represents the line of best fit.

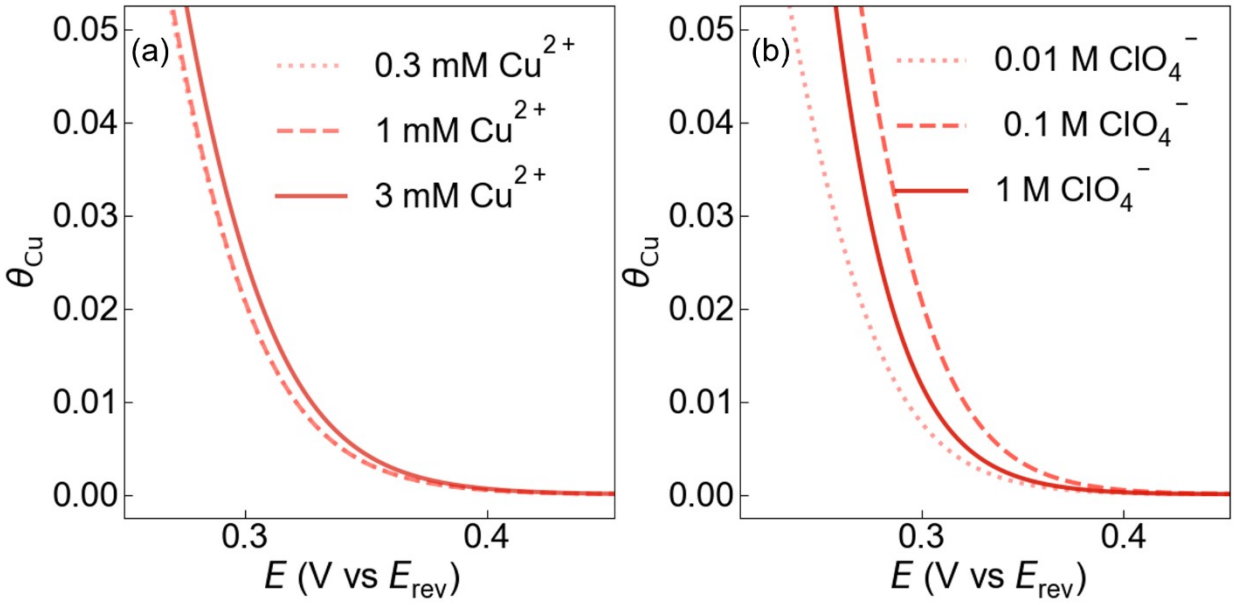

Figure S15: Adsorption isotherm fit to the Frumkin adsorption isotherm of Cu coverage vs the reversible deposition potential for (a) Cu^{2+} in 0.10 M ClO_4^- with interaction parameters of g = 7.4(2), 6.6(6), 7.1(2) for $[Cu^{2+}]$ = 0.0003, 0.001, 0.01 M respectively. (b) ClO_4^- in 0.001 M Cu^{2+} with interaction parameters of g = 13(4), 6.6(6), 2.9(1) for $[ClO_4^-]$ = 0.01, 0.1, 1.0 M, respectively.

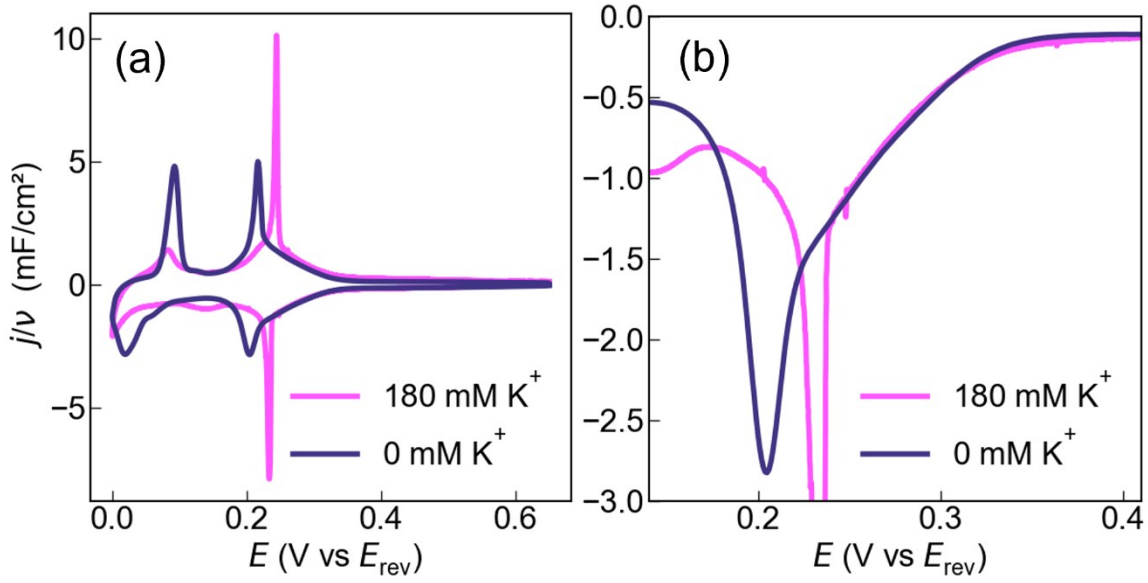

Figure S16: Voltammetry of annealed Au(111) electrodes in 1 mM CuO, 0.010 M H_2SO_4, and 0.090 M K_2SO_4 (pink) and 1 mM CuO, 0.100 M H_2SO_4 (blue) showing (a) the difference in peak current for each trace and (b) the different potential at which the peak occurs. All traces are at 10 mV s^{-1}.

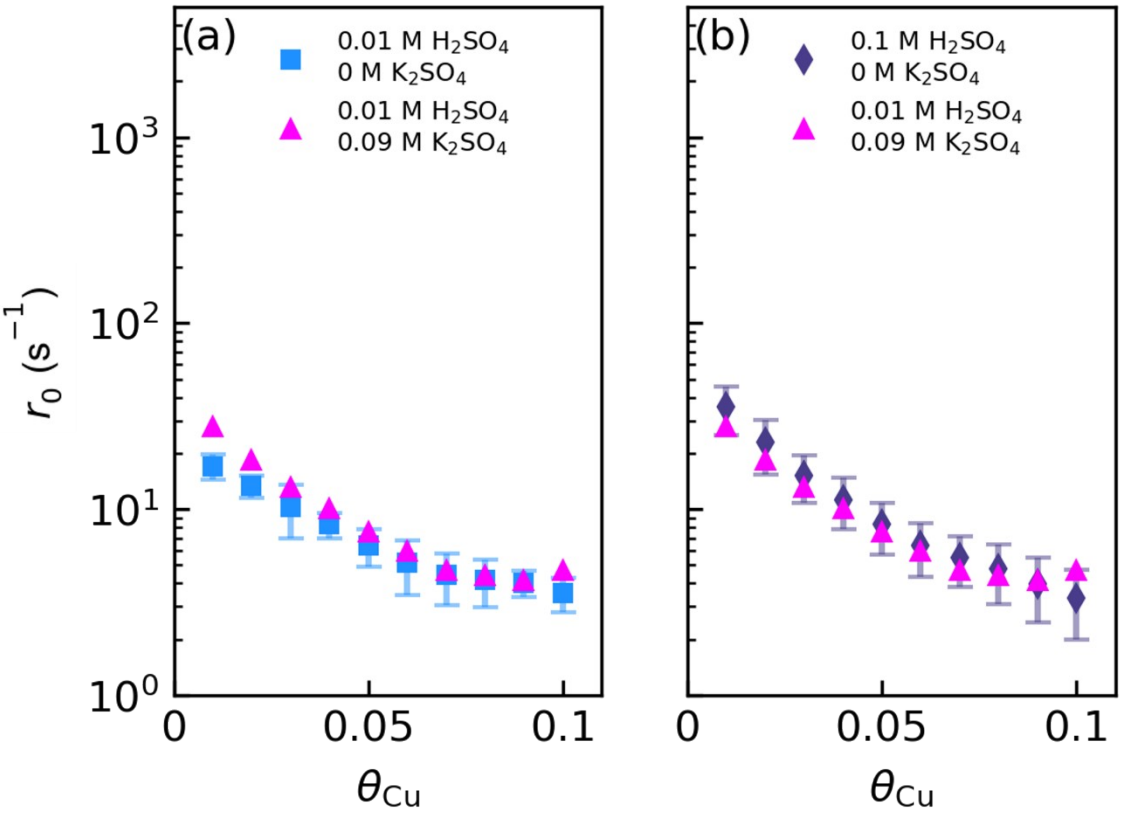

Figure S17: Coverage dependence for r_0 Au(111) in 1 mM CuO, 0.01 M H_2SO_4, and 0.09 M K_2SO_4 (pink) compared to 1 mM CuO in (a) 0.01 M H_2SO_4 and (b) 0.1 M H_2SO_4.

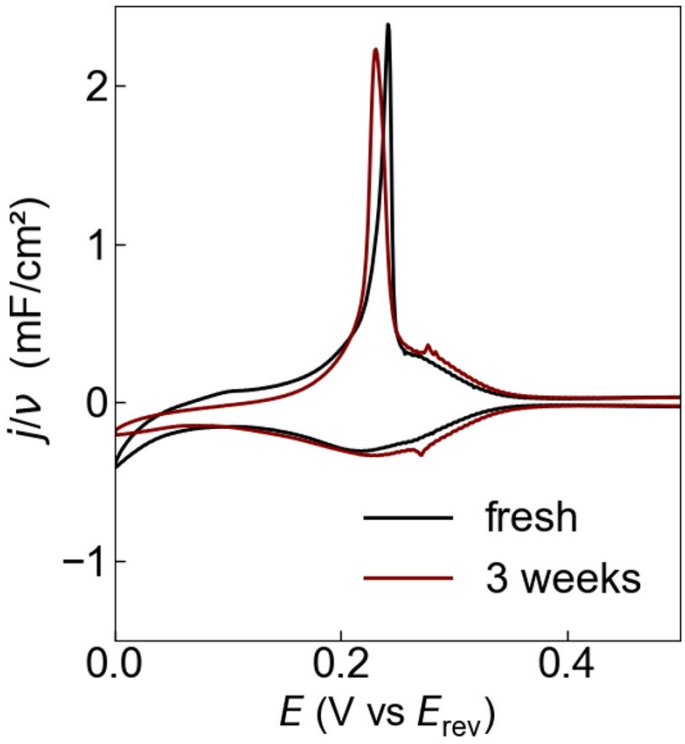

Figure S18: CV of 10 mM Cu^{2+} dissolved in 0.1 M ClO_4^- on Au(111) at 25 mV s^{-1}. The black trace shows the response of a fresh Au(111) electrode tested within 2 days of preparing the electrolyte. The red trace represents the response of a fresh Au(111) in the same electrolyte after 3 weeks of resting at room temperature.

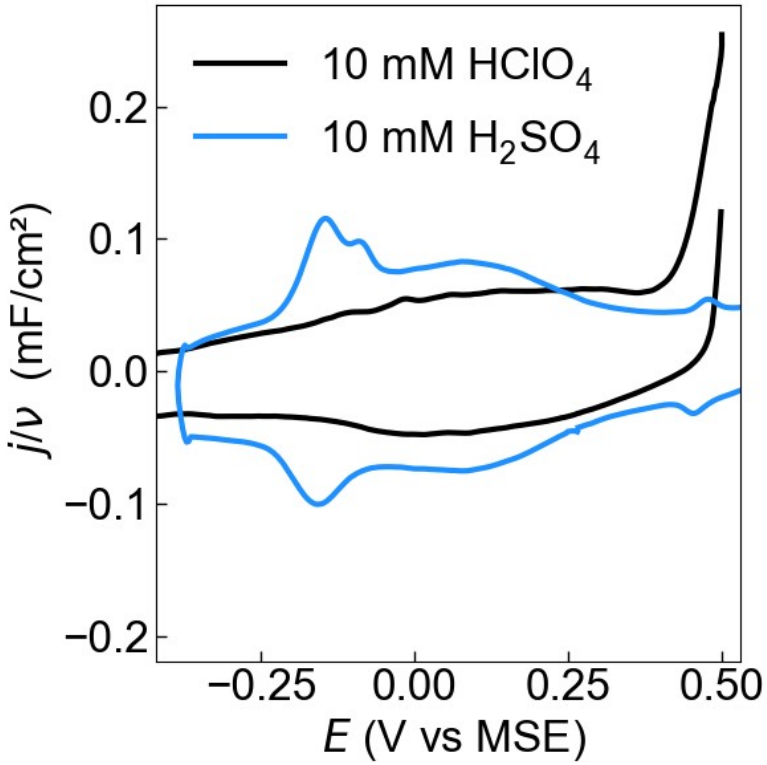

Figure S19: CV of Au(111) in 10 mM $HClO_4$ (black) and 10 mM H_2SO_4 (blue) normalized to scan-rate (25 mV s^{-1}).

Supplementary References:

(1) Bard, A. J.; Faulkner, L. R.; White, H. S. *Electrochemical Methods: Fundamentals and Applications*; John Wiley & Sons, 2022.
(2) Kuo, D.-Y.; Lu, X.; Hu, B.; Abruña, H. D.; Suntivich, J. Rate and Mechanism of Electrochemical Formation of Surface-Bound Hydrogen on Pt(111) Single Crystals. *J. Phys. Chem. Lett.* **2022**, *13* (27), 6383–6390. https://doi.org/10.1021/acs.jpclett.2c01734.
(3) Pinto, L. M. C.; Spohr, E.; Quaino, P.; Santos, E.; Schmickler, W. Why Silver Deposition Is so Fast: Solving the Enigma of Metal Deposition. *Angew. Chem. Int. Ed.* **2013**, *52* (30), 7883–7885. https://doi.org/10.1002/anie.201301998.
(4) Kang, R.; Zhao, Y.; Hait, D.; A. Gauthier, J.; A. Kempler, P.; A. Thurman, K.; W. Boettcher, S.; Head-Gordon, M. Understanding Ion-Transfer Reactions in Silver Electrodissolution and Electrodeposition from First-Principles Calculations and Experiments. *Chem. Sci.* **2024**, *15* (13), 4996–5008. https://doi.org/10.1039/D3SC05791G.
(5) Bockris, J.; Enyo, M. Mechanism of Electrodeposition and Dissolution Processes of Copper in Aqueous Solutions. *Trans. Faraday Soc.* **1962**, *58*, 1187–1202.
(6) Gerischer, Heinz. Mechanism of Electrolytic Deposition and Dissolution of Metals. *Anal. Chem.* **1959**, *31* (1), 33–39. https://doi.org/10.1021/ac60145a007.